Angular Correlation Functions of High p_{T} Charged Hadrons in pp, PbPb, and pPb Collision Monte-Carlo Simulations

an Honors Thesis

by

Gabriel Bonilla

under the supervision of

Dr. Manuel Calderón de la Barca Sánchez

at

UNIVERSITY OF CALIFORNIA, DAVIS

May 27, 2014

Abstract

The quark-gluon plasma has a role in understanding the strong force, which is described by the theory of quantum chromodynamics. To probe the quark-gluon plasma, heavy ions are collided at high energies to recreate the conditions present in the early universe. Experiments like the Compact Muon Solenoid (CMS) at the Large Hadron Collider examine the results of colliding heavy nuclei together at high energies to recreate the quark gluon plasma. One such observation is jet quenching, which is believed to occur when the jets of particles produced in the collision interact with the plasma and lose energy. In this study, we use the PYTHIA, HYDJET (Hydrodynamics plus Jets) and UrQMD (Ultrarelativistic Quantum Molecular Dynamics) Monte-Carlo simulation programs to observe how the angular correlations of the jets of particles created in collisions vary across the choice of collision system (proton-proton, proton-lead, lead-lead). We will also look at the behavior of these angular correlations to help us understand the mechanisms of energy loss.

Acknowledgements

I would like to acknowledge ...

Dr. Manuel Calderón de la Barca Sánchez for being my mentor and teacher,

Rylan Conway for being my trustworthy graduate student mentor,

Dr. Daniel Cebra for always giving me hard questions to answer,

My friends at UCDNPG,

My friends at the Physics Club,

My friends from McNair,

My friends from Lowell,

and my friends at family at home for always believing in me.

I'm not done yet! But I've made good progress.

Contents

1 Introduction

Physics is the study of the interactions between the various kinds of matter and energy which inhabit the univserse. Experiments involving matter and energy are carried out in order to determine the nature of their interaction, and theories are constructed from the results in an attempt to predict the outcome of future experiments. In the developement of physics, four fundamental forces have been identified: the strong force, the weak force, the electromagnetic force, and the gravitational force. Quantum descriptions of the weak and electromagnetic force have been developed and unified in an electroweak theory, while similar descriptions of gravity have remained elusive. This thesis will concern itself with attempts to develop the theory of the strong force, quantum chromodynamics (QCD).

The Large Hadron Collider (LHC) at CERN is physics' largest attempt, in terms of both physical size and energy scale, to understand the strong force. It is a particle accelerator which collides protons and heavy ions together at high energies in order to probe their finer structure. The energies involved reach several teraelectronvolts (TeV) per nucleon and allow physicists to test theories such as the standard model and supersymmetry. In particular, the standard model predicted the Higgs boson, whose existence was detected at the LHC. In order to detect new particles whose rapid decay prohibits direct observation, physicists must rely on the detected properties of the stable decay products that the detector collects. These properties include energy,

momentum, charge, and position, which are then used to recover details of the initial nature of the collision. Recovering such details is a fruitful way in itself to study the nature of the forces involved in the collision. Ultimately, we hope to reach a complete understanding of the strong force.

Experimental data is later compared with theoretical predictions to gauge physicists understanding of the underlying theory. These predictions come in the form of Monte-Carlo (MC) simulations. MC simulations generate events through random number generation in order to model probabilistic phenomena. In this thesis we will be looking at the MC predictions from the PYTHIA, HYDJET, and UrQMD event generators, which simulate the proton-proton (pp), lead-lead (PbPb), and proton-lead (pPb) collision systems, respectively. Specifically, we will be examining the angular correlation functions they produce. First, we describe the detector geometry with respect to which we will be constructing our coordinate system upon which we make our measurements.

1.1 The Detector Geometry

This thesis will model its analysis of angular correlation functions after similar analyses [1] [2] done using data collected with the CMS dectector. Therefore, we wil be modeling our coordinate system after the geometry of the CMS detector.

The CMS detector is most easily characterized as a barrel shape. As such, it suggests the use of a cylindrical coordinate system. We denote the the z-

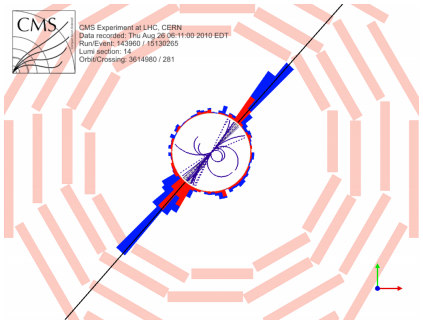

Figure 1: This pp collision event display from CMS highlights the radial symmetry of the ϕ coordinate. The high towers demonstate where jets showered onto the detector, in clear accordance with the conservation of momentum.

axis to be the beam axis, with $z = 0$ at the center of the collision, and ϕ to be the azimuthal angle. Remark: given the radial symmetry of the detector and the coordinate, we are free to define the location on the detector where $\phi = 0$ to be any convenient location. Borrowing from spherical coordinates, we also adopt an addition angular coordinate, θ, the polar coordinate with respect to the z-axis, with $\theta = 0$ along the beam axis. Unique to particle physics is the psuedorapidity coordinate η, another angular coordinate which is defined as a function of θ as follows: $\eta = -\ln \tan(\theta/2)$ [1]. This thesis will concern itself primarily with measurements involving the η and ϕ coordinates of particles. Using the coordinate system defined above, we may describe the range of the CMS detector: 0 to 2π in ϕ, and -2.4 to 2.4 in η.

1.2 The Proton-Proton Collision System

The proton is a hadron which is composed of three quarks bound together by gluons. Collectively, we call these constituents partons. Quarks and gluons

have color charge, which means that they cannot exist as free particles. In proton-proton (pp) collisions, these partons may be ejected at high energies. Due to color confinement, increasing the distances between colored objects increases the energy density of the color field between them. This energy will be suffient to create quarks and gluons out of the vacuum. This process is known as hadronization and leads to highly collimated showers of particles called jets which are ultimately what we detect [3].

Due to the initial state of the system having negligible net transverse momentum, conservation of momentum dictates that that final state of the system have near zero net transverse momentum as well. In dijet events in which two high p_T jets are produced, these jets will shower onto the detector in opposite directions, leading to an angular ϕ separation ($\Delta\phi$) of π between the two jets as seen down the beam axis (Fig 1). In this situation the jets are said to be back-to-back. The construction of the η coordinate system does not lend itself as nicely to back-to-back angular separations; back-to-back jets can have any $\Delta\eta$ separation while still conserving momentum. When constrained to lie within the CMS detector, $\Delta\eta$ can range between -4.8 to 4.8.

1.3 The Lead-Lead Collision System

The lead ion is a nucleus composed of 208 nucleons, 82 of which are protons. In lead-lead ($PbPb$) collisions, there are many more interacting partons and collective matter effects become important. Two effects unseen in

pp collisions distinguish *PbPb* angular correlation functions from that of *pp* collisions: jet quenching and collective flow. These two effects result from a relatively new phenomenon: the quark gluon plasma (QGP). At sufficiently high energies, constituent quarks and gluons are not confined to nucleons. Instead, partons experience asymptotic freedom due to the high amount of color-charged particles. This results in a near-perfect fluid [4] and the system can be studied hydrodynamically.

1.3.1 Jet Quenching

As in *pp* collisions, dijet events also occur in *PbPb* collisions. In *pp* collisions, the ejected partons escaped into free space in a symmetric fashion, and their reconstructed energies after hadronization are comparable. However, in *PbPb* collisions, the QGP created provides an additional medium through which the jets must traverse. Before hadronization, the ejected partons and QGP are both color-charged, and as such interact with each other, causing the ejected parton to lose energy. This loss of energy will result in fewer particles produced during hadronization, and thus a smaller jet, hence the name jet quenching (Fig. 2). Dijet events can spawn anywhere within the QGP, which leads to an asymmetry in quenching between the two jets depending on which ejected parton has to travel through more QGP.

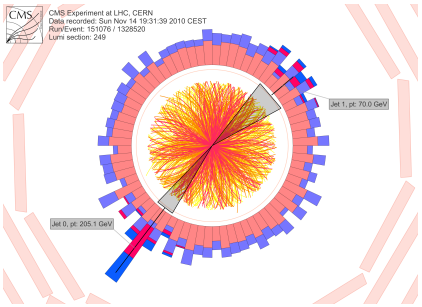

Figure 2: This PbPb collision event display from CMS highlights an asymmetry in the towers, providing evidence for jet quenching.

1.3.2 Collective Flow

Lead ions are large enough such that we may define an impact parameter $\vec{b}$, the vector designating the center-to-center distance between the two colliding nuclei. $PbPb$ collisions occur at various $|\vec{b}|$ values, and each one leads to a different QGP configuration (Fig. 3). For $|\vec{b}| \approx 0$ collisions, the lead ions are nearly head on, resulting in symmetric QGP formation. For $|\vec{b}| > 0$ collisions, the lead ions are off-center and the nuclear overlap region resembles an almond shape along the reaction plane, which is defined by the beam axis and the impact parameter [5]. The asymmetric shape of the almond gives rise to pressure gradients which will in turn have a direct affect on the pattern of particles showered onto the detector. More precisely, the asymmetry of the pressure gradiants in the QGP will give rise to an asymmetry in the transverse momentum as a function of ϕ. As ϕ is a periodic coordinate, we may quantify this asymmetry in the form of a Fourier expansion over ϕ, with the n^{th} Fourier coefficient being denoted as v_n [5]. These flow coefficients

will make themselves apparent in angular correlation functions created from $PbPb$ collisions if the event generator includes flow as part of its model.

1.4 The Proton-Lead Collision System

Proton-lead (pPb) collisions were proposed as a control to study whether or not initial nuclear conditions from $PbPb$ collisions have an effect on jet quenching [6]. Not much is known about pPb collisions in comparison to those of pp and $PbPb$. In this thesis, we will attempt to synthesize what is learned about pp and $PbPb$ collisions to make a prediction as to how pPb collision systems behave. One previous hypothesis is that the nuclear overlap is too small to produce a QGP and thus too small to produce flow effects, which may or may not be true. Additionally, one expects that the presence of more nucleons in the pPb system over the pp system to introduce transverse momentum via scattering, resulting in final particles in a broader distribution about π in $\Delta\phi$, whereas in pp collisions particles largely scattered in a narrow distribution about π in $\Delta\phi$, due to the minimal transverse momentum present in the system. However, as will be discussed later in the thesis, data suggest that something is present to cause the system to behave oppositely from what is expected, indicating a lack of understanding of the pPb collision system. Morever, angular correlation functions produced from data from CMS have significant v_2 and v_3, which as of yet has no explanation [1].

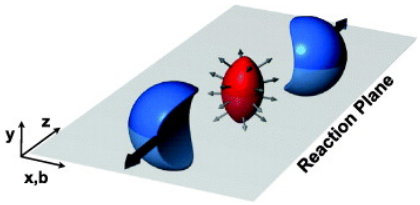

Figure 3: This PbPb collision illustration shows the almond shaped QGP formed after an off-center collision. Image from Snellings [5].

1.5 Event Generators

In this thesis, we consider data collected from event generators such as PYTHIA, HYDJET, and UrQMD. Event generators, in general, are computational models designed to simulate actual particle collisions. Parameters such as beam energy, collision system, and number of events can be set, and the generator will output an according list of particles produced in the collision. Consequently, the three stages of user interaction with the event generator can be summarized as follows: Initialization, in which the user sets the collision parameters, Event Looping, in which the user has access to event-level information, and Particle Looping, in which the user has access to particle-level information within a single event.

1.5.1 PYTHIA

PYTHIA, specifically, PYTHIA 8.1, is the event generator created by Torbjörn Sjöstrand et al [7]. It is written in C++ and can handle pp, $p\bar{p}$, $e\bar{e}$, and $\mu\bar{\mu}$ collisions; we will be considering pp collisions. Pythia generates its events in three stages: process generation, multi-parton interactions, and hadronisa-

tion and decay [7]. In particular, PYTHIA simulates hadronization through a model known as the Lund string Model, which works by modeling color force fields between partons as a string between the two that has fixed energy per unit length [8]. As the partons separate, the strings break apart into hadrons, modelling fragmentation and hadronization. Through the Lund string model coupled with decay processes, this is how PYTHIA determines its final particles.

1.5.2 HYDJET

HYDJET (HYDdrodynamics plus JETs), specifically, HYDJET++, is a heavy ion event generator created by Igor Lokhtin et al [9]. It is built on top of PYTHIA 6.4 and PYQUEN 1.5 (PYthia QUENched), a PYTHIA modification to model jet-quenching [10]. It is also coupled with HYDRO from the first version of HYDJET, the event generator used to simulate flow effects [11]. In summary, HYDJET is loosely a superposition of PYTHIA collisions modified by flow effects and jet quenching, which are precisely the differences we see between pp and $PbPb$ collisions.

1.5.3 UrQMD

UrQMD (Ultrarelativistic Quantum Molecular Dynamics), is another heavy ion event generator, in this case, "a microscopic transport model in which hadrons are propagated on classical trajectories" [12]. As a transport model, UrQMD does not explicitly model global effects such as collective flow or jet

quenching. This is consistent with the idea that a QGP does not form in a pPb collision.

2 Objective

In this thesis, we will explore the *angular correlation function* (ACF) plots constructed from data generated by the PYTHIA, HYDJET, and UrQMD generators in an attempt to understand the pp, $PbPb$ and pPb collision systems. The ACFs will be calculated at various p_T ranges and will be done using the C++ programming language in the ROOT environment. Angular correlation functions are used in order to explore the spatial distribution of the final particles after a collision. In particular, the angular differences between all the particles created in an event will be plotted, which illustrates the relative prevalence of certain angular separations over others. We may immediately predict that the prescence of jets will leave a signature on the ACFs due to their characteristic separation, but finer details such as how these signatures change as a function of transverse momentum and collision system is something that will be explored in this thesis.

Through these angular correlation functions, we hope to verify that the notions used to characterize each collision system such as jets, jet quenching, collective flow, and soft scattering are indeed present in the manner in which they are described. We also aim to provide an appraisal of the ACFs as they vary over the choice of collision system and transverse momentum.

Ultimately, from our study, we hope to make a prediction in order to test our understanding of the pPb collsion system. Therefore, we include an additional study on the pPb collision system using data collected from the CMS detector in order to determine whether or not the explanation event generators give for pp and $PbPb$ phenomena can be synthesized to provide an explanation for pPb phenomena.

3 Methods

3.1 Angular Correlation Functions

The Angular Correlation Function (ACF): A constructed C++ program will generate the object of this analysis, the ACF, from the data collected from event generators. The ACF is a 2-dimensional histogram of the angular differences between all possible pairings of particles over an event cumulated over many events. The characteristic features of the ACF are its peak at $(\Delta\eta,\Delta\phi) = (0,0)$, denoting a large multiplicity of pairs of particles with small angular separation, as well as a bump at $(\Delta\eta,\pi)$, denoting a multiplicity of pairs of particles with back-to-back angular separation, spread out over . As the structure of the ACF is very qualitative in nature, we supplement this analysis by calculating quantities that will allow us quantify how the ACF varies as a function of transverse momentum.

3.2 Initialization

In generating the data we employ to construct angular correlation functions, we resort to the event generators PYTHIA, HYDJET, and UrQMD. In general, they need only be set up with a beam energy parameter and collision system, and the event generator is ready to began outputting event lists. These lists collect the particles created after such an event, including information on their momentum, energy, charge, and particle type. Once the user is able to access these lists, one is able to write a C++ program to loop over each particle created in the event and begin filling histograms of their properties.

3.3 Signal Correlation Function

3.3.1 Description

The signal correlation function is an explicit characterization of the relative angular separation of particles produced in a single event. Particles are correlated with particles from the same event and many events are taken as it is assumed any individual collision is the same as any other collision up to impact parameter. Hence, it is appropriate to sum correlations over many events for stronger statistics. After running a simulation of a desired number of events, the signal ACF is constructed by filling an appropriate histogram with the angular separation and between two particles in a pair for every possible pair in that event. In addition to the restriction of correlating

particles within the same event, we also impose the restriction that particle pairs fall within certain tranvserse momentum ranges that we designate as the trigger particle momentum ($p_T^{trigger}$) range and the associated particle momentum (p_T^{assoc}) range.

3.3.2 Motivation

The motivation behind these two ranges is the notion that jets are characterized by their leading particle, known as the trigger particle, that carries the most momentum, followed closely by other particles, known as associated particles, which have slightly less momentum [1]. As a result, possible pairs are determined by looking at the particles of a single event that fall in a certain p_T^{assoc} and $p_T^{trigger}$ range. When considering trigger particles and associated particles, every particle pair we look at will be a particle from a trigger particle bin compared against a particle from an associated particle bin. Given that the trigger and associated particle bins are based on different p_T ranges, we never have to worry about comparing a particle against itself, which would result in a separation identically zero.

3.3.3 Explanation of Features

The peak at S(0,0) results from the geometry of a jet in that a jet is a cone of particles that are close together (Fig 4.). The smaller peak that forms at 2π radians and is actually spread out over η results from the geometry of back-to-back jets in that they are composed of particles that are π radians from

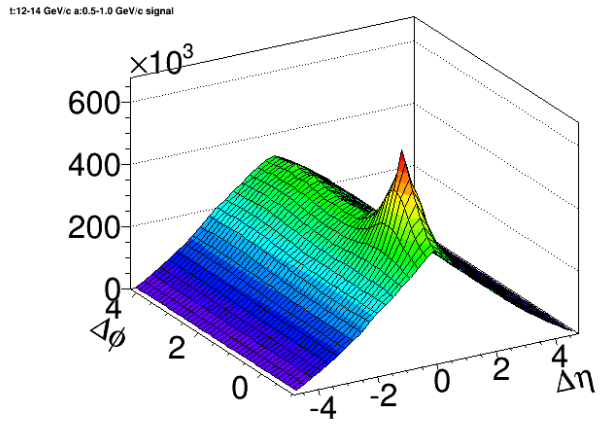

Figure 4: This is an example of a signal angular correlation function (denoted by S($\Delta\eta$,$\Delta\phi$)) created using pp event data from PYTHIA at a beam energy of $\sqrt{s} = 2.76$TeV. In this case, the p_T ranges chosen are $0.5 < p_T^{assoc} < 1.0$ and $12 < p_T^{trigger} < 14$.

each other in $\Delta\phi$ but can take on any value in $\Delta\eta$. The triangular background over the $\Delta\eta$ axis is a result of detector acceptance: If only particles that fall into the range -2.4 to 2.4 in η are accepted, there are many pairs that can fall in that range that can have a $\Delta\eta$ of 0 between them. However, if a particle pair that has a $\Delta\eta$ of 4.8 is desired, one particle at 2.4 and another particle at -2.4 is needed, a condition very few particle pairs satisfy. This explains why the triangular shape in $\Delta\eta$ has a peak at 0 and drops off as it approaches 4.8 and -4.8. This same behavior is actually also seen in the $\Delta\phi$ axis if one restricts the ϕ values to be between two values like 0 and π, 0 and 2π, -π and π, and so on, for the same reason. However, a separation of $\Delta\phi$ is equivalent to a separation of $\Delta\phi + 2\pi$, which is not satisfied if the

ACF falls off at the edges. For this reason, we require that the histogram be periodic in $\Delta\phi$. Plotting pairs with $\Delta\phi$ in addition to pairs with $\Delta\phi$ $\pm 2\pi$ satisfies this periodicity requirement. In essence, we are taking the original triangular structure with a peak at zero and now adding two more triangular structures that are shifted plus and minus 2π. This will result in a flat structure in $\Delta\phi$ from -2π to 2π. $\Delta\phi$ and $\Delta\eta$ are also affected by the fact that a pair with a separation of ($\Delta\phi$,$\Delta\eta$) can also be said to have a separation of ($\Delta\eta$,$\Delta\phi$), ($-\Delta\eta$,$\Delta\phi$), ($\Delta\eta$,$-\Delta\phi$), or ($-\Delta\eta$,$-\Delta\phi$), depending on the order in which the angles $\phi_1, \phi_2; \eta_1, \eta_2$ are subtracted. In order to counteract this, we impose signless separation and fill only one quadrant of the ACF. We fill the remaining three quadrants by reflection, keeping in mind the periodicity requirement in $\Delta\phi$.

3.4 Background Correlation Function

3.4.1 Description

The background correlation function is an explicit characterization of the relative angular separation of particles produced in a single event excluding jet physics. Particles are correlated with particles from ten different events. For stronger statistics, we continue extracting correlations with a selection of eleven additional events, one of which will be correlated against the other ten. After collecting a desired number of events, the background ACF is constructed by filling an appropriate histogram with the angular separation

and between two particles in a pair for every possible pair across events. In addition to the restriction of correlating particles in different events, we also impose the restriction that particle pairs fall within certain $p_T^{trigger}$ and p_T^{assoc} ranges. In fact, the event which is correlated against the ten others is the event in which trigger particles are taken, and the ten used for correlation are the events in which associated particles are taken.

3.4.2 Motivation

The peaks at 0 and π radians in $\Delta\phi$ in the signal ACF provide evidence for jet phenomena. If we were to take particle pairs among different events, the fact that there is no preferred ϕ value for jets to shoot off in would result in a random distribution of $\Delta\phi$ values. However, there is a remaining preferred structure in η and $\Delta\eta$ due to non-jet physics, such as particle production, and the detector acceptance, as well as random combinatorial effects. The goal of the background ACF is to illustrate non-jet physics so that it may be later divided out. The signal ACF is a combination of jet physics and non-jet physics. Given that we want to study the consequences of jet physics, we want to eventually produce a plot illustrating solely jet physics. This is accomplished by taking particle pairs across events. By construction, it is now impossible to find a pair of particles that belong in a single jet and thus all evidence of jets should be nonexistent in the background ACF. The remaining angular correlation structure is that which arises from other physical effects, which we should remove if we wish to

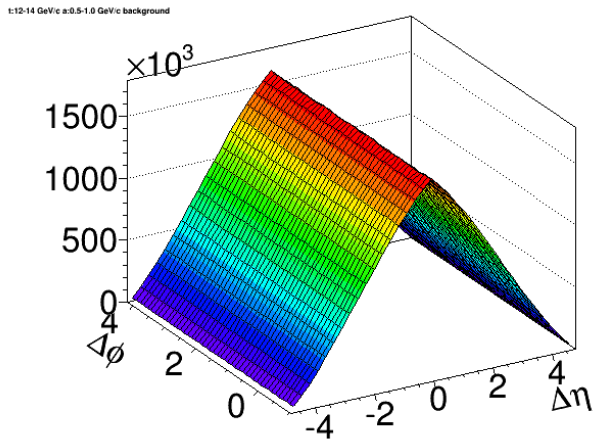

Figure 5: This is an example of a background angular correlation function (denoted by B($\Delta\eta$,$\Delta\phi$)) created using pp event data from PYTHIA at a beam energy of $\sqrt{s} = 2.76$TeV. In this case, the p_T ranges chosen are $0.5 < p_T^{assoc} < 1.0$ and $12 < p_T^{trigger} < 14$.

examine only the effects of jets on the ACF.

3.4.3 Explanation of Features

The structure of the background 2D angular correlation histogram is that which is flat in $\Delta\phi$, due to the construction of pairs with random ϕ. However, the $\Delta\eta$ structure from the signal plot remains (Fig. 5). The $\Delta\eta$ structure is very nearly triangular, but in fact has two inflection points. This is a result of the non-jet physics we wish to remove from our signal plot to more closely examine the effects of jet physics. We will then take the previous signal plot and divide it by the created background plot to create the resulting divided plot. It is in this plot where we can see the effects of jet-physics.

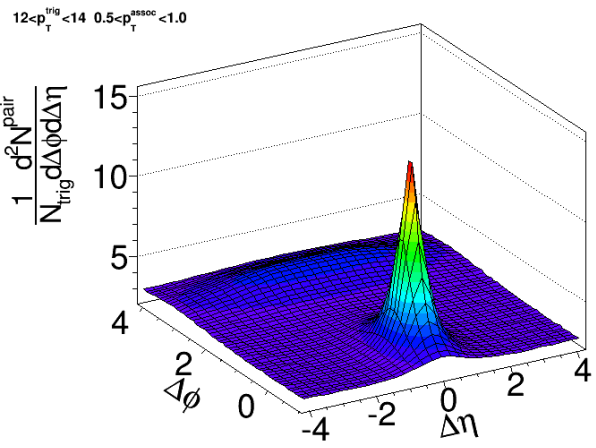

Figure 6: This is an example of a divided angular correlation function created using the previous signal and background ACFs, which used pp event data from PYTHIA at a beam energy of $\sqrt{s} = 2.76$TeV. As in the previous cases, the p_T ranges chosen are $0.5 < p_T^{assoc} < 1.0$ and $12 < p_T^{trigger} < 14$.

3.5 Divided Correlation Function

Once the signal ACF and background ACF are obtained, a divided ACF may be constructed (Fig. 6). The full description for the divided ACF is given by (1), where N_{trig} and $B(0,0)$ serve for normalization [1].

$$\frac{1}{N_{trig}} \frac{d^2N^{pair}}{d\Delta\eta d\Delta\phi} = B(0,0) \times \frac{S(\Delta\eta, \Delta\phi)}{B(\Delta\eta, \Delta\phi)} \tag{1}$$

Once the divided plot is obtained, the first task is to normalize the divided plots in order to compare them among different analyses that have a different number of events. The normalization is done by scaling the divided plot by the number of trigger particles in the trigger bin, denoted by N_{trig}, to

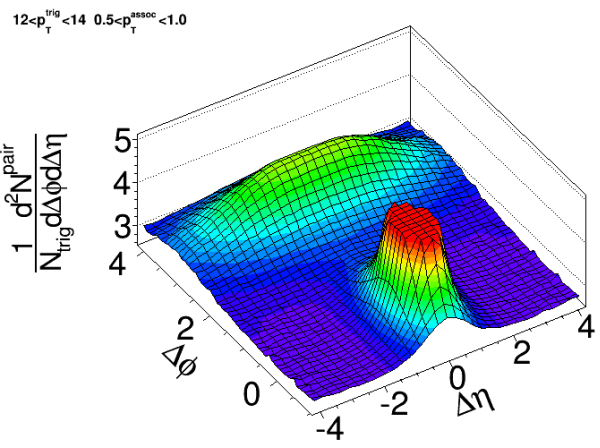

Figure 7: This is a truncated version of the previous divided angular correlation function created using the previous signal and background ACFs, which used pp event data from PYTHIA at a beam energy of $\sqrt{s} = 2.76$TeV. As before, the p_T ranges chosen are $0.5 < p_T^{assoc} < 1.0$ and $12 < p_T^{trigger} < 14$.

obtain a "per-trigger-particle" plot. We also multiply by the height of the background at B(0,0) to negate the scaling effects that resulted from dividing by the background plot in the previous section. In order to more clearly see the structure at the back end of the divided ACF, we truncate the plot at a suitable height (Fig. 7). After all ACFs are obtained, further analysis may be done on slices of the two-dimensional histogram. This will allow quantitative measurements across the $(\Delta\eta, \Delta\eta)$ space of the ACF.

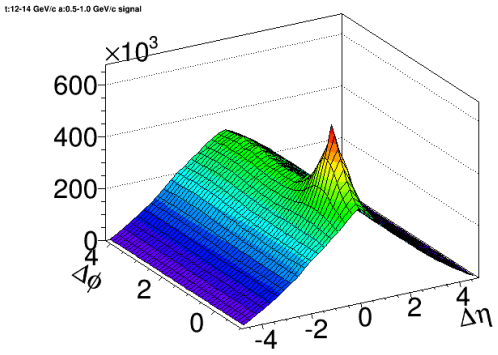

Figure 8: This is the signal angular correlation function created using pp event data from PYTHIA at a beam energy of $\sqrt{s} = 2.76$TeV. In this case, the p_T ranges chosen are $0.5 < p_T^{assoc} < 1.0$ and $12 < p_T^{trigger} < 14$ The near-side peak from jet phenomenon is clearly visible.

4 Results

4.1 Conclusions of Angular Correlation Functions

Analogous procedures were carried out in order to obtain divided ACFs from HYDJET and UrQMD. We list the signal ACF, background ACF, and divided ACF here. For convenience, we repeat the pp ACFs. We also describe the phenomena thought to be illustrated in each plot.

PYTHIA ACFs were constructed by generating one million events and correlating them as in the Methods section. $p_T^{trigger}$ ranges were chosen to lie between 12 and 14, 14 and 20, 20 and 30, and 30 and 50GeV. p_T^{assoc} ranges were chosen to lie between 0.5 and 1, 1 and 2, 2 and 3, 3 and 4GeV, and 4 and 6GeV. Different p_T ranges were chosen for the HYDJET and UrQMD ACFs as their p_T falls off too fast to have meaningful statistics at high p_T.

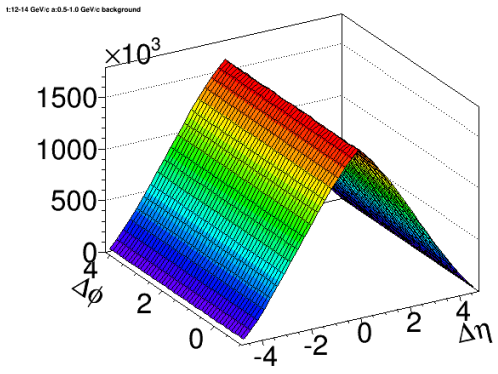

Figure 9: This is the background angular correlation function created using pp event data from PYTHIA at a beam energy of $\sqrt{s} = 2.76$TeV with the p_T ranges chosen as $0.5 < p_T^{assoc} < 1.0$ and $12 < p_T^{trigger} < 14$.

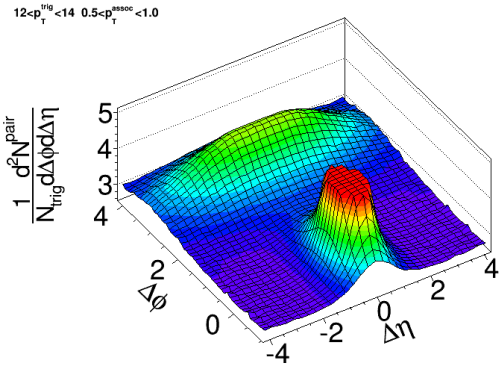

Figure 10: This is the divided angular correlation function created using the previous signal and background ACFs, which used pp event data from PYTHIA at a beam energy of $\sqrt{s} = 2.76$TeV. As in the previous cases, the p_T ranges chosen are $0.5 < p_T^{assoc} < 1.0$ and $12 < p_T^{trigger} < 14$. The high peak from jet phenomenon and the broad bump from back-to-back jet phenomenon are visible here. One million PYTHIA events were used in the generation of this plot.

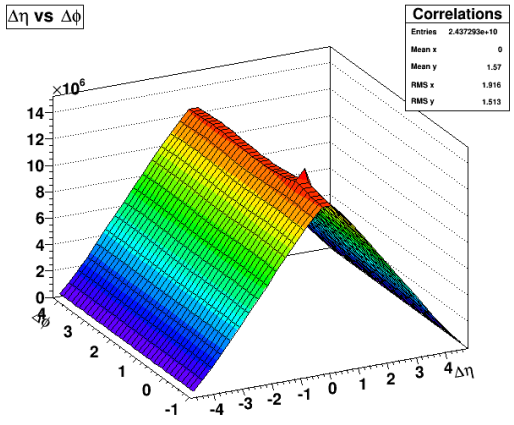

Figure 11: This is the signal angular correlation function created using *PbPb* event data from HYDJET at a beam energy of $\sqrt{s} = 2.76$TeV. There is now a much strong triangular structure in the signal ACF compared to the *pp* signal ACF. This is due to the presence of many more final particles, the majority of which are not produced with jet effects, which can be clearly seen here. A small wave-like modulation can be seen at the top of the structure.

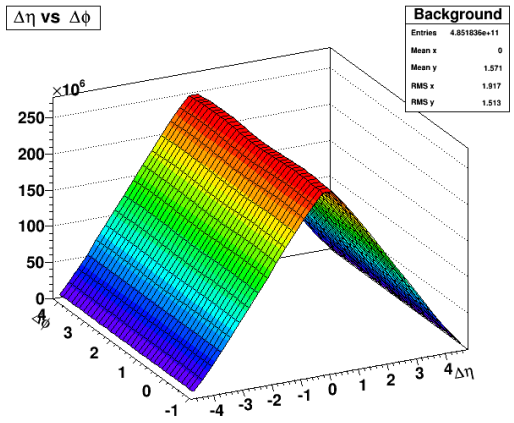

Figure 12: This is the background angular correlation function created using *PbPb* event data from HYDJET at a beam energy of $\sqrt{s} = 2.76$TeV. By construction, all evidence of jet effects has been eliminated. However, the modulation of $\Delta\phi$ remains, indicating a non-jet origin to this phenomenon.

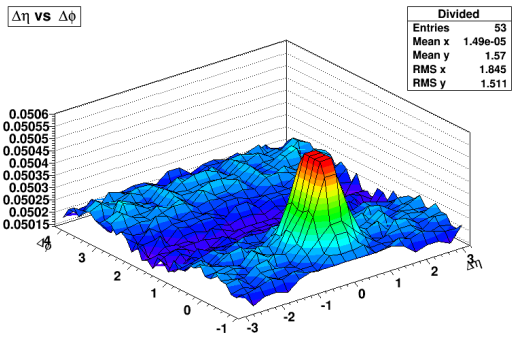

Figure 13: This is the divided angular correlation function created using the previous signal and background ACFs, which used $PbPb$ event data from HYDJET at a beam energy of $\sqrt{s} = 2.76$TeV. The $\Delta\phi$ modulation of non-jet origin is still present in the final ACF, indicating the effect of the collision on the angular separation of jets. In this case, jet quenching is present as there is no visible far-side bump in addition to the modulation. This is a result of HYDJET including jet quenching in its model.

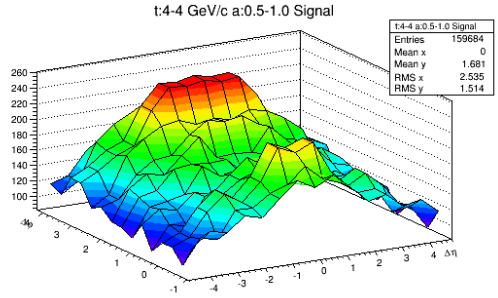

Figure 14: This is the signal angular correlation function created using pPb event data from UrQMD at a beam energy of $\sqrt{s} = 5.02$TeV, which was chosen to replicate a previous study done on pPb collisions at this energy [1]. The lack of statistics is a result of the difficulty of gathering events. However, we can already begin to notice the weaker triangular shape when compared to $PbPb$ collisions. This is a result of the fewer amount of particles produced in a pPb collision. A peak at the origin hints towards jet phenomena, but the large structure at the back does not usually overpower the peak in that case.

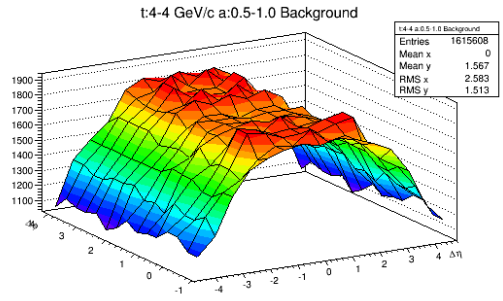

Figure 15: This is the background angular correlation function created using pPb event data from UrQMD at a beam energy of $\sqrt{s} = 5.02$TeV. By construction, all evidence of jet effects has been eliminated. However, a structure not previously seen in either pp or $PbPb$ collisions is present here: a large plateau structure in $\Delta\eta$ instead of the usual triangular shape. This necessitates phenomena that spread particles out in $\Delta\eta$ in pPb collisions, and may be characteristic of the "ridge effect," although UrQMD does not particularly model for that.

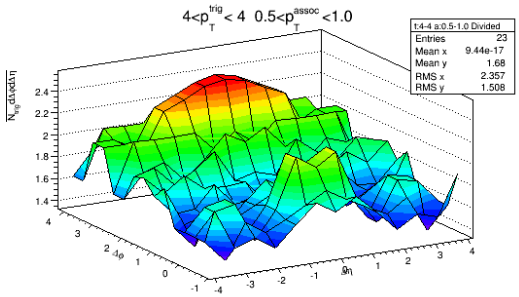

Figure 16: This is the divided angular correlation function created using the previous signal and background UrQMD ACFs, and uses a $3 < p_T^{trigger} < 4$ and $0.5 < p_T^a ssoc < 1$. The $\Delta\eta$ at the back remains, indicating either the lack of jet quenching or the lack of jets altogether, given its size relative to the peak at the origin. However, more statistics are needed before anything is concluded.

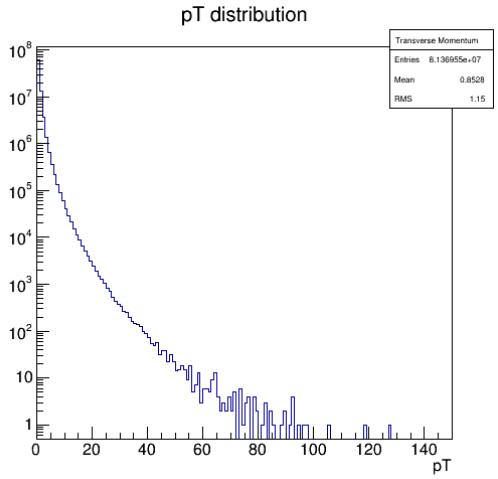

Figure 17: This figure shows the tranverse momentum distribution of the final particles in one million pp collisons in PYTHIA at a beam energy of $\sqrt{s} = 2.76$TeV. In this case, the PYTHIA parameter pTHatMin, which sets the minimum invariant transverse momentum, was set to 100GeV.

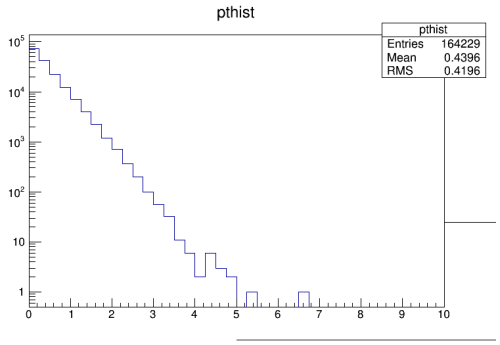

Figure 18: This figure shows the tranverse momentum distribution of the final particles in one hundred $PbPb$ collisons in HYDJET at a beam energy of $\sqrt{s} = 2.76$TeV. It is clear that this p_T distribution falls off faster than that of pp, which necessitated the changing of the trigger and associated bin ranges. This is also evidence of the thermalization that happens as a result of the QGP present in $PbPb$ collisions.

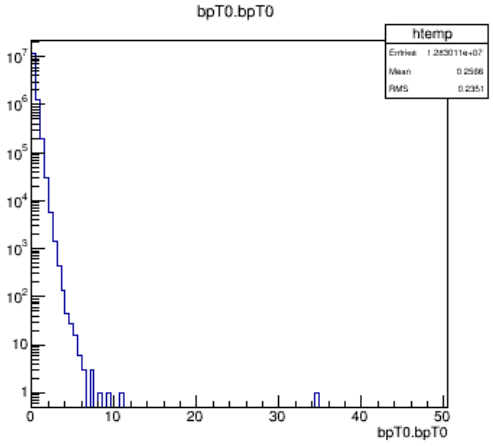

Figure 19: This figure shows the transverse momentum distribution of the particles present in forty-thousand pPb collisions in UrQMD at a beam energy of $\sqrt{s} = 5.02$TeV. The p_T distribution here also falls off too quickly to use high $p_T^{trigger}$ and p_T^{assoc} particle ranges. This may be a result of the incident proton losing too much energy to the lead nucleus' constituent particles.

4.2 Results of ZYAM Analysis

Further analysis involved calculating zero-yield-at-minimum (ZYAM) yields for the pp system. Once the normalized ACF is obtained, a quantative value known as the associated yield can be calculated. This is first done by finding the ZYAM point. ZYAM points are found on projections of $\Delta\eta$ slices of the normalized ACF, also known as correlated yields [1]. The ZYAM point is a $\Delta\phi$ value, which corresponds to the point of minimum multiplicity. It is found by finding the minimum of a fitted second-degree polynomial to the region between the two $\Delta\phi$ peaks. This range is from 1.1 to 2 on the $\Delta\eta$-axis. In constructing our associated yield, we set the yield to be zero at the ZYAM point by construction. The associated yield is then obtained by integrating

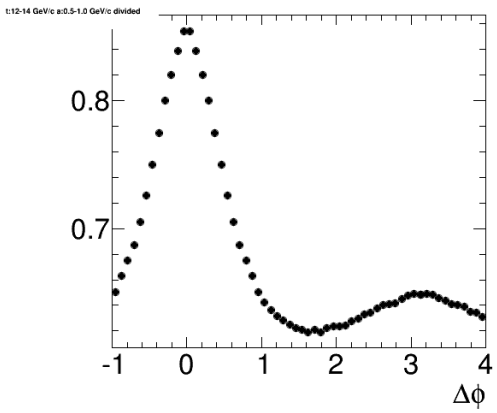

Figure 20: This figure is a projection of a slice (correlated yield) of the *pp* ACF shown earlier. In this case, the slice taken is $0 < |\Delta\eta| < 1$. The characteristic jet peak is clearly visible at $\Delta\phi = 0$, while the back-to-back peak is also noticable at $\Delta\phi = \pi$. Note: This plot is before ZYAM subtraction.

the 1D histogram from 0 up to the ZYAM point. This allows us to obtain an associated yield value per 2D plot per $\Delta\eta$ slice. Doing multiple slices, we can obtain many associated yield values as we move from the short-range region (-1 to 1 in $\Delta\eta$ to the long-range region (the region outside of -2 to 2 in $\Delta\eta$). This allows us to have a quantitative characterization of the ACFs created earlier.

4.3 An Attempt to Characterize the pPb System

In addition to the analyses done on ACFs produced by event generators, an analysis was also done on pPb data collected by the CMS detector [1]. As per our obtained understanding of collision systems, *pPb* collisions differ from those of *pp* most clearly because of the difference in the number of

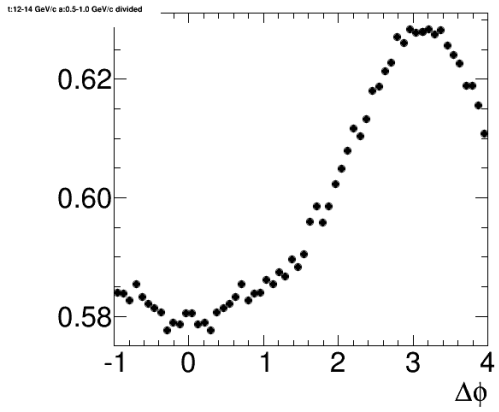

Figure 21: This figure is a correlated yield of the pp ACF shown earlier. In this case, the slice taken is $2 < |\Delta\eta| < 3$. The jet peak at $\Delta\phi = 0$ is no longer visible, while the back-to-back peak is remains prominent at $\Delta\phi = \pi$. This is an indication that the near-side jet peak only lives within a small range of $\Delta\eta$, while the away-side back-to-back structure lives within a broad range of $\Delta\eta$. Note: This plot is before ZYAM subtraction. Notice that the back-to-back structure does not get any taller; it is below 0.7 in both the short-range ($0 < |\Delta\eta| < 1$) projection and in the long-range ($2 < |\Delta\eta| < 3$) projection.

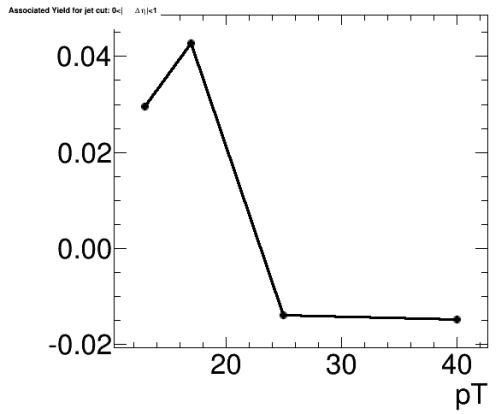

Figure 22: This figure is a plot of the short-range associated yield as a function of $p_T^{trigger}$. The yield falls off due to the lack of trigger particles at higher p_T.

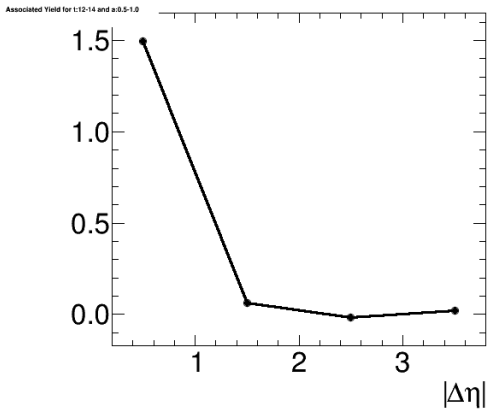

Figure 23: This figure is a plot of the associated yield as a function of $|\Delta\eta|$ slice. The yield falls off due to the majority of the particles are close together in η due to jet phenomena in the pp system.

interacting nucleons. In pp collisions, back-to-back jet phenomena is a clear consequence of the conservation of momentum (Fig. 1). However, in the presence of multiple nucleons, the lead nucleus has many nucleons whose inherent transverse momentum can be transferred to the incident proton in the form of scattering. Back-to-back phenomenon is no longer a consequence of conservation of momentum. Back-to-back phenomena was the reason for the sharp away-side ($\Delta\phi = \pi$) structure in the pp ACFs (Fig. 10). However, in collisions with additional nucleons, such as in the case of pPb, there is no need for back-to-back phenomenon anymore. Hence, it is expected that the away-side structure will broaden about $\Delta\phi = \pi$ as a result of these additional interactions. In fact, one may conclude that the more interactions there are, the more the initial transverse momentum distribution should become randomized, and the more the distribution of the separation of particles in

$\Delta\phi = \pi$ should broaden out. Given that the multiplicity of particles produced is roughly proportional to the amount of scatterings which occur in the pPb system, we quantify this prediction via the following statement: The width of the away-side structure of the projected pPb ACF about $\Delta\phi = \pi$ increases as a function of multiplicity. We assess our prediction in the discussion section of this thesis.

5 Discussion

For the most part, the ACFs created using the event generators PYTHIA and HYDJET match with their counterparts constructed from data detected at the CMS detector; the phenomena described earlier in this thesis is an adequate description of pp and $PbPb$ collsion systems. In the case of UrQMD the statistics are still too poor to be able to tell. However the low energy regime for which UrQMD was designed will probably dictate that ACFs generated from its data will be in poor agreement with experiment. ZYAM analysis done on the the pp ACFs are also in agreement with the behavior that jet phenomena dictate. ZYAM analysis will need to be done on $PbPb$ ACFs as well in order to say the same for HYDJET. In the case of $PbPb$ ACFs however, the not-jet modulation in $\Delta\phi$ will need to be accounted for. Due to the wave-like nature of the modulation, a fourier expansion over $\Delta\phi$ is proposed. It appears that the fourier expansion will involve the same flow coefficients described earlier, and is a direct result of the collective flow which

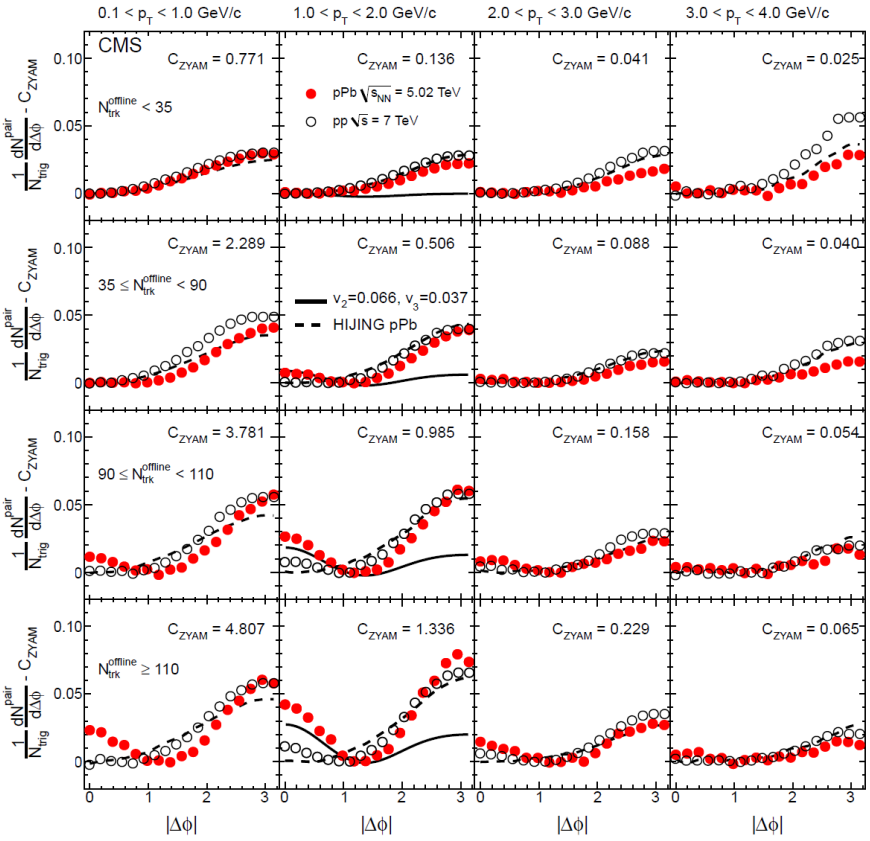

Figure 24: This figure reproduces that which was published by the CMS collaboration in [1]. It is a plot of projected pPb ACFs as a function of both multiplicity and p_T. Their caption is as follows: "Correlated yield obtained from the ZYAM procedure as a function of $|\phi|$ averaged over $2 < |\eta| < 4$ in different p_T and multiplicity bins for 5.02 TeV pPb data (solid circles) and 7 TeV pp data (open circles). The p_T selection applies to both particles in each pair. Statistical uncertainties are smaller than the marker size. The subtracted ZYAM constant is listed in each panel. Also shown are pPb predictions for hijing [24] (dashed curves) and a hydrodynamic model [25] (solid curves shown for $1 < p_T < 2$ GeV/c)." [1]

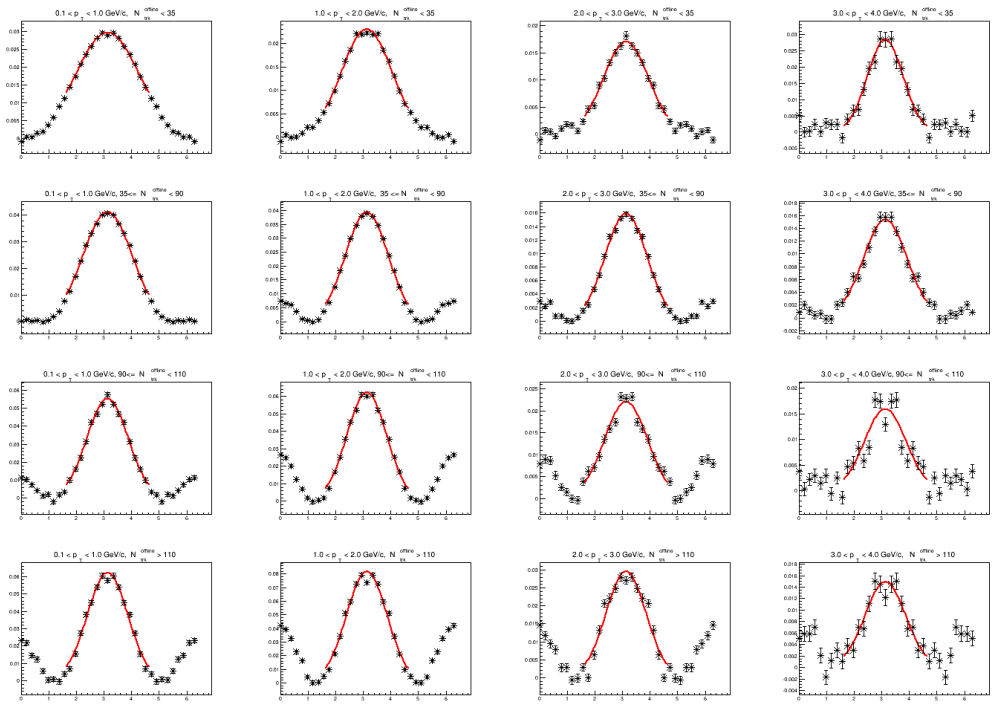

Figure 25: Here the sixteen graphs from above are reproduced and reflected due to the symmetry about π. A gaussian is fit to the range $(\pi - 1.5, \pi + 1.5)$. Their widths correspond to the widths of the away side structure of CMS's pPb ACF in $\Delta\phi$.

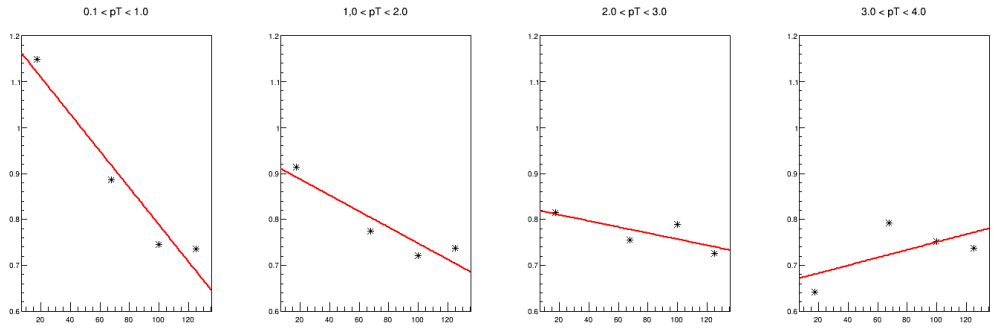

Figure 26: These four plots summarize the above sixteen by plotting the width of the gaussian as a function of multiplicity. Each graph corresponds to a different transverse momentum range. It is immediately clear that the width of the gaussian follows an inverse relationship with multiplicity, which is the opposite of what was expected.

HYDJET specifically models [5][9].

The analysis done on the pPb correlated yields from CMS has yielded unexpected results. As mentioned earlier, pPb collision systems were predicted to have an away-side structure that broadens as a function of multiplicity, reflecting the increase in scattering needed to reach that multiplicity. However, as was found, the away side structure behaves oppositely to what was predicted; the away-side structure becomes tighter about $\Delta\phi = 0$ as multiplicity increases. This cannot be explained with the same reasoning that was used for the pp collision system, as jets should spread in $\Delta\phi$ after each collision. In addition, in a large system such as that of pPb, the majority of the particles produced are not from jet effects. This indicates that other collective effects need to be accounted for in the pPb system. One may note the wave-like pattern is similar to the one of $PbPb$ ACFs, which was a result of

HYDJETs collective flow effects used to replicate quark-gluon plasma effects. It remains to be seen whether it is reasonable to conclude that a quark-gluon plasma may also be formed in a much smaller pPb system. For now it can be said that our understanding of pPb collisions remain incomplete.

However, even PYTHIA, modeling the simplest collision system, seems to be imcomplete. In pp ACFs with high multiplicity, a near side "ridge" becomes present, which as of yet lacks explanation[1]. This incompleteness in the pp model clearly translates to incompleteness of the pPb and $pBpB$ models, as they are based off of the simpler pp model. This will have to be accounted for in future event generators and perhaps point toward new physics phenomenon. In the ridge effect, particles originally near in $\Delta\eta$ begin to spread out. This indicates the prescence of an interaction that changes their momentum. This same method of analysis was done in order to conclude that the pPb collision system is not entirely understood either. In summary, more study with both event generators and CMS data is necessary before the pPb system can be said to be understood, even at a rudimentary level.

6 Conclusion

This purpose of this study was to examine the structure of angular correlation functions and extract qualitative information which helps us explain the phenomena involved with different collision systems. The addition of $PbPb$ and pPb ACFs helped us compare across all collision systems to determine

which effects persist, and to what degree. It is clear that not all effects are present across all event generators, and that event generators need to be additionally supplemented in order to model other effects, as in the case of HYDJET with jet quenching and collective flow. The results of the pPb analysis led us to conclude that pPb phenomena is unlike either the smaller pp system or the larger $PbPb$ system; it cannot be explained as any combination of effects present in both pp and $PbPb$. As a result, it is necessary to collect data from the CMS detector for all three systems for a full understand of how pp phenomena change as more and more nucleons are involved in the collision.

Future study will involve a focus on pPb systems over those of pp and pPb to determine how effects from pp and $PbPb$ are present in pPb as well as how effects present in neither may manifest themselves in pPb collision. Future study will also involve close comparisons of yet additional event generators to real data collected from CMS in order to determine the ranges at which the model prediction begins to deviate from experiment. In addition, it is hoped that an understanding of pPb systems is reached.

References

[1] V. Khachatryan et al. (CMS Collaboration), JHEP 1009, 091 (2010). [arxiv:1009.4122 [nucl-ex]]

[2] CMS Collaboration collaboration, S. Chatrchyan et. al., JHEP 1107 (2011) 076 [arXiv:1105.2438 [nucl-ex]]

[3] E. Norrbin and T. Sjostrand, Production and hadronization of heavy quarks, Eur.Phys.J. C17 (2000) 137–161, [arxiv:0005110[hep-ph]]

[4] U. W. Heinz, [arXiv:0512051v1[nucl-th]]

[5] Raimond Snellings 2011 New J. Phys. 13 055008 doi:10.1088/1367-2630/13/5/055008

[6] B. Abelev et al. (ALICE Collaboration), Phys. Rev. Lett. 110, 082302 (2013).

[7] T. Sjostrand, S. Mrenna and P. Z. Skands, Comput. Phys. Commun. 178, 852 (2008) [arXiv:0710.3820 [hep-ph]].

[8] B. Andersson et al. (2002). [arxiv:0212122[hep-ph]]

[9] I.P. Lokhtin, L.V. Malinina, S.V. Petrushanko, A.M. Snigirev, I. Arsene et al., Comput. Phys. Commun. 180, 779 (2009). [arxiv:0809.2708[hep-ph]]

[10] I.P. Lokhtin and A.M. Snigirev, Eur.Phys.J. C45, 211 (2006). [arxiv:0506189[hep-ph]]

[11] I. P. Lokhtin and A. M. Snigirev. (2003). [arxiv:0312204[hep-ph]]

[12] M. Bleicher, E. Zabrodin, C. Spieles, S. A. Bass, et al., J. Phys. G: Nucl. Part. Phys. 25, 1859 (1999). [arXiv:9909407[hep-ph]]